Viscosity and Thermal Conductivity of Stable Graphite Suspensions Near Percolation

Citation: Ma, Lei, Jianjian Wang, Amy M. Marconnet, Alexander C. Barbati, Gareth H. McKinley, Wei Liu, and Gang Chen. "Viscosity and Thermal Conductivity of Stable Graphite Suspensions Near Percolation." Nano Lett. 15, no. 1 (January 14, 2015): 127–133.

As Published: http://dx.doi.org/10.1021/nl503181w

Publisher: American Chemical Society (ACS)

Persistent URL: http://hdl.handle.net/1721.1/100774

Version: Author's final manuscript: final author's manuscript post peer review, without publisher's formatting or copy editing

Viscosity and Thermal Conductivity of Stable Graphite Suspensions Near Percolation

Lei Ma[1, 2, *], Jianjian Wang[2, *], Amy M. Marconnet[2, 3], Alexander C. Barbati[2], Gareth H. McKinley[2], Wei Liu[1], Gang Chen[2,†]

1. School of Energy and Power, Huazhong University of Science and Technology, Wuhan 430074, P.R. China

2. Department of Mechanical Engineering, Massachusetts Institute of Technology, 77 Massachusetts Avenue, Cambridge, Massachusetts 02139, United States

3. School of Mechanical Engineering, Purdue University, West Lafayette, Indiana 47907, United States.

Abstract:

Nanofluids have received much attention due, in part, to the range of properties possible with different combinations of nanoparticles and base fluids. In this work, we measure the viscosity of suspensions of graphite particles in ethylene glycol as a function of the volume fraction, shear rate, and temperature below and above the percolation threshold. We also measure and contrast the trends observed in the viscosity with increasing volume fraction to the thermal conductivity behavior of the same suspensions: above the percolation threshold, the slope that describes the rate of thermal conductivity enhancement with concentration reduces compared to below the percolation threshold, whereas that of the viscosity enhancement

* These authors contributed equally to this work.
† Corresponding author: gchen2@mit.edu

increases. While the thermal conductivity enhancement is independent of temperature, the viscosity changes show a strong dependence on temperature and exhibit different trends with respect to the temperature at different shear rates above the percolation threshold. Interpretation of the experimental observations is provided within the framework of Stokesian dynamics simulations of the suspension microstructure, and suggest that although diffusive contributions are not important for the observed thermal conductivity enhancement, they are important for understanding the variations in the viscosity with changes of temperature and shear rate above the percolation threshold. The experimental results can be collapsed to a single master curve through calculation of a single dimensionless parameter (a Péclet number based on the rotary diffusivity of the graphite particles).

Key words: percolation, viscosity, shear thinning, graphite suspensions

Colloidal solutions with well-dispersed nanoparticles, also called nanofluids,[1] have attracted extensive attention due to their abnormal thermal conductivity enhancement and the potential applications in energy technologies.[2-8] Heat conduction in nanofluids has been extensively studied,[9-16] and the variation in results has led to much debate as to the mechanisms of thermal conduction in nanofluids. By freezing nanofluids consisting of

alumina nanoparticles in different base fluids, Gao et al.[16] demonstrated that clustering is a key factor for enhancing the thermal conductivity. Zheng et al.[17] observed peculiar percolation phenomena in the thermal conductivity for stable graphite suspensions. Below the percolation threshold, the thermal conductivity increases faster with increasing graphite loading than above the percolation threshold, which is directly in contrast with the electrical conductivity results. Combined with AC impedance spectroscopy studies, they interpreted this observation that there is an abrupt reduction in the slope of the thermal conductivity enhancement after percolation as most likely related to the role of the interfacial energy of the particle clusters before and after percolation. These studies established that Brownian motion and diffusive contributions were not responsible for the experimentally observed thermal conductivity enhancement.

The rheology of nanofluids and suspensions is another important material property for practical applications,[18-25] especially for flow-based application such as all kinds of coolants in the pipe cooling systems. For simple Newtonian fluids (water, ethylene glycol, etc.), the shear viscosity is solely a function of temperature, and is independent of the shear rate. However, for non-Newtonian fluids such as polymer melts, blood, and ketchup, the shear viscosity is not only a function of temperature, but also a

function of the shear rate and shear history.[26-31] Past work has shown that the steady shear viscosity $\eta(\dot{\gamma}, T)$ of nanofluids typically decreases with increasing temperature at a fixed shear rate.[32-37] Although the viscosity of suspensions has been extensively studied in the literature,[21, 37-42] there have been few studies that focus on thermal effects on the macroscopic suspension viscosity when the volume loadings pass from the dilute regime into the percolated regime. In this work, we measure the thermal conductivity and viscosity of graphite suspensions as a function of temperature and volume fraction, focusing on the percolation behavior. We observe two distinct trends for thermal conductivity and viscosity below and above percolation. From our analysis of the experimental data, we conclude that a diffusive Brownian contribution of the dispersed colloidal structures remains important in the measured viscosity above the percolation threshold despite its insignificance for the thermal conductivity.

Graphite flakes are first prepared by sulphuric acid intercalation, which exfoliates the natural graphite into graphite flakes, and then expanded via microwave radiation.[17, 43-45] The expanded graphite flakes are then mixed with ethylene glycol. The suspensions are ultrasonicated for 35 mins to disperse the particles and to form stable graphite dispersions. Samples of different volume fraction are prepared by diluting the concentrated 1 vol. %

suspension ensuring the graphite flakes are from the same fabrication batch for all samples. The SEM image in Figure 1(a) reveals the typical morphology of the graphite flakes. The individual graphite particles have diameters of several micrometers, but, as can be observed from the optical microscope image shown in Fig. 1(b), the flakes form much larger clusters. The clusters are isolated from each other when the graphite volume fraction is low (typically less than $\phi < 0.07$ vol. %), and merge to form a percolation network when the graphite volume fraction is high (typically higher than $\phi \geq$ 0.1 vol. %).[17, 46] Our previous studies based on electrical conductivity, AC impedance spectroscopy, and thermal conductivity measurements have established that such nanofluids have a percolation threshold around $\phi_c \approx$ 0.07% volume fraction for an ethylene glycol based dispersion.

The viscosity of the graphite dispersion at room temperature is measured using a controlled stress rheometer (TA Instruments AR-G2) with a cone-and-plate geometry. The viscosity results show good repeatability; during repeated measurements with the same suspension the viscosity curves coincide with each other with standard deviation less than 2%. Two key trends of viscosity with shear rate are evident in Fig. 2. First, the viscosity of the graphite suspension increases as the volume fraction increases. Second, the graphite suspension exhibits non-Newtonian behavior. Specifically, the

viscosity decreases with increasing shear rate (i.e. the dispersion is shear thinning), and the level of shear thinning increases for higher volume fractions. This is likely due to the graphite clusters and flakes preferentially realigning themselves along the flow direction under the application of an imposed shear stress. This structural reorganization reduces particle-particle interactions and, thus, reduces the viscosity.

In a previous paper,[17] some of the present authors observed that the thermal conductivity of graphite suspensions increases more rapidly with concentration below the percolation threshold than above percolation. To further study this effect, we measured the thermal conductivity of the samples (following a similar preparation protocol as introduced in our previous paper[17]) used in the rheological characterization and the results are shown in Fig. 3a. Note that below the percolation threshold (around 0.07 vol. %), the thermal conductivity increases faster than above the percolation threshold, consistent with our previous report.[17, 46] Through prior AC impedance spectroscopy studies, we determined that this effect is due to tighter contact between individual graphite flakes below the percolation threshold, which arises as a result of energy minimization of isolated graphite clusters.[17] In contrast to the thermal conductivity trend, the viscosity of the graphite suspensions increases much more rapidly after percolation than before

percolation, as shown in Fig. 3b. In addition, the viscosity dependence is well fitted with the Doolittle equation[47] $\eta(\phi) = \mathrm{A}\exp\left(\mathrm{B}\frac{\phi}{\phi_f}\right) = \mathrm{A}\exp(\mathrm{B}'\phi)$ (Fig. 3c), rather than the weaker power law dependence (Fig. 3d) observed for the electrical conductivity.[17, 46] Here A and B are numerical constants and ϕ_f is the free-space volume fraction of the suspension which is close to unity in our case since the particle volume fraction ϕ is less than 1%.

The effects of temperature on the thermal conductivity and viscosity of suspensions can provide further clues to the mechanisms behind the volume fraction dependence, in addition to the importance of these properties for practical applications. The thermal conductivity of the suspension is measured by the transient hotwire method, which is a quite accurate and standard method for liquid thermal conductivity measurement with uncertainty about $\pm$1%. As shown in Fig. 4, as the temperature varies from room temperature to 65℃, the enhancement in thermal conductivity does not vary significantly. This is consistent with the conclusion that Brownian motion of the dispersed particles is not responsible for the observed thermal conductivity enhancement in the nanofluids.[46, 48-50]

The effect of temperature on the viscosity of nanofluids and suspensions, however, is more complex than its effect on the thermal conductivity. Figures 5(a)-(c) show the steady shear viscosity of several graphite suspensions as a

function of shear rate at different temperatures and Figs. 6(a)-(f) plot the data to clearly show the temperature dependence of viscosity at different volume fractions and three selected values of the imposed shear rate. As the temperature increases from room temperature to 65 ℃, the viscosity of the dilute suspensions, which show Newtonian behavior, is significantly reduced. Above the percolation threshold, the results are more complex (Fig. 5c) and the variation with temperature is non-monotonic. We explore this complex thermo-rheological response in greater detail in Fig. 6.

For dilute suspensions, the viscosity decreases with increasing temperature within the measured shear rate range [Figs. 6(a)-(c)], similar to that of the pure solvent. At low shear rates, the viscosity depends strongly not only on temperature, but also on the volume fraction (Fig.6a). However, at higher shear rates, the variation in the viscosity between different volume loadings is reduced as the particles are increasingly shear-aligned [*cf*. Figs. 6(b) and 6(c)]. For concentrated suspensions, more interesting phenomena appear [Figs. 6(d)-(f)]. The viscosity is found to increase with increasing temperature (Fig. 6d) at low shear rates but then change to the reverse behavior at high shear rates [Fig. 6(f)].

To understand the thermo-rheological behavior of these nanofluids, we first consider the temperature-dependence of the suspending solvent. The

pure solvent viscosity $\mu_s(T)$ can be described by a thermally rate-activated process of Arrhenius type so that $\mu_s(T) = \mu_0 \exp\left[\frac{\Delta H}{R}(\frac{1}{T} - \frac{1}{T_0})\right]$, [51] where R is the ideal gas constant, ΔH is the energy barrier for the solvent molecules to make a transition from an original energy state to a new energy state under imposed shearing, and μ_0 is the viscosity of the solvent at the reference temperature T_0. This leads to a decrease in the viscosity of the solvent with increasing temperature.[52-54] Regression to the pure ethylene glycol data in Fig. 6a gives $\frac{\Delta H}{RT_0} = 9.977$, $\mu_0 = 0.0147\text{Pa} \cdot \text{s}$ at $T_0 = 300\text{K}$.

The rheology of concentrated suspensions has been studied extensively.[55-59] Brady and co-workers[60-64] have developed a Stokesian dynamics approach that is widely used to predict the microstructural properties and macroscopic properties of hard-sphere suspensions. Although the dispersed graphite flakes are not hard spheres, we found that our experimental data can be rationalized using ideas from Stokesian dynamics simulations when combined with understandings of the structures of the graphite flakes in the suspension. In particular the observation that the graphite flakes are closely aggregated into isolated clusters below the percolation threshold due to global surface energy minimization while above

the percolation threshold, the contact between flakes weakens, as supported by our previous AC impedance studies.[17, 46]

The relevant dimensionless parameter when discussing relative contributions to the viscosity of a Brownian dispersion or suspension viscosity is the Péclet number $Pe = \tau_D/\tau_S$ which relates the characteristic diffusive timescale τ_D of the dispersed phase to the characteristic flow timescale τ_S. A large Péclet number means that the applied shearing deformation dominates while a small Péclet number means Brownian motion is dominant. The characteristic convective timescale at a given imposed shear rate $\dot{\gamma}$ is $\tau_S = 1/\dot{\gamma}$. The characteristic timescale for diffusion is $\tau_D \sim a^2/D$, where a is the Stokes radius of the particle, and D is the translational diffusion coefficient. The diffusion coefficient can be calculated from the well-known Einstein relation $D = \frac{k_B T}{f}$, where f is the friction coefficient, and this relation is valid for arbitrary shape particles. For spherical particle with radius a, $f = 6\pi\mu(T)a$ and $\tau_D = \frac{6\pi\mu(T)a^3}{k_B T}$. Thus the Péclet number for spherical particles is $Pe = \frac{6\pi\mu(T)\dot{\gamma}a^3}{k_B T}$. As the temperature increases, the characteristic timescale for Brownian motion reduces since $\frac{\mu(T)}{T}$ decreases and the Péclet number decreases. For nonspherical particles, the more relevant dimensionless parameter is a rotational Péclet number, in which τ_D

is the characteristic timescale of particle reorientation caused by Brownian motion. If we approximate the shape of graphite flakes as circular disks with diameter $2a$, then $\tau_D = \frac{32\mu(T)a^3}{3k_BT}$ and the Péclet number becomes $Pe = \frac{32\mu(T)\dot{\gamma}a^3}{3k_BT}$.[65] Note that both the translational and rotational Péclet numbers have similar functional forms and are proportional to $\frac{\mu(T)\dot{\gamma}a^3}{k_BT}$ (where a^3 is proportional to the particle hydrodynamic volume), and the difference lies only in the numerical prefactor. Since our graphite flakes are neither spherical particles nor perfect circular disks, we neglect the specific value of the numerical prefactor when calculating the Péclet number for our system as it simply shifts the magnitude of Péclet number by a constant factor. For dilute suspensions, as inferred from prior works on the same system, the graphite flakes are quite tightly aggregated into isolated clusters[17]. In this dilute regime, we should consider these isolated clusters, not individual graphite flakes, as the relevant Brownian objects. Note that the typical size of a graphite cluster observed via optical microscopy is on the order of ~100μm, which is two orders of magnitude larger than the lateral size of an individual graphite flake so that the hydrodynamic volume of the cluster is about 6 orders of magnitude larger than the flake volume. The large graphite cluster size, which gives a relatively large Péclet number, indicates the

insignificance of Brownian motion on the motion of the clusters even at low imposed shear rates. As the shear rate is increased, the contribution of Brownian motion to the total viscosity of the clustered dispersion becomes increasingly negligible, as indicated by the smaller and smaller difference between different volume loadings (Figs. 6b and 6c).

For more concentrated suspensions, the graphite clusters merge together and form a sample-spanning percolation structure. The driving force to minimize the surface energy of isolated clusters become smaller thus the contact between graphite flakes become looser, as supported by our AC impedance spectroscopy studies reported in a previous study.[17] This reduced contact allows individual graphite flakes increasing freedom to diffuse. Brownian motion of individual graphite flakes thus becomes more important in the percolated regime, especially when the imposed shear rate $\dot{\gamma}$ is sufficiently low.

To quantitatively understand the inverted trends of the viscosity observed in Fig. 6d and 6f for samples above the percolation threshold, we plot the viscosity of concentrated suspensions as a function of the Péclet number for several characteristic shear rates in Fig. 7. To calculate the Péclet number, we estimate the average flake lateral size $2a$ observed in SEM to be on the order of ~1μm so that $a^3 \sim 10^{-18}\text{m}^3$. In our experiments, the Péclet

number can be varied by changing not only the shear rate $\dot{\gamma}$, but also temperature via the Arrhenius thermal dependence of $\mu(T)$ for the ethylene glycol solvent. In Fig. 7, the Péclet number variation is due to the temperature change since the shear rate is held fixed in each subfigure. When the shear rate is small ($10\mathrm{s}^{-1}$), the flow is in the low Péclet number regime (Fig. 7a), and diffusive contributions dominate the suspension viscosity. As a consequence even though the temperature rise causes a decrease of the solvent viscosity, the measured suspension viscosity still increases with the increasing temperature. However, when the shear rate is high ($1000\mathrm{s}^{-1}$), the Péclet number is orders of magnitude higher and the total dissipation in the system is now dominated by locally advective hydrodynamic effects (Fig. 7c). The Brownian motion of graphite flakes becomes much less important and hence the suspension viscosity closely follows the solvent viscosity trend as the temperature is increased.

The transition from Brownian-motion dominated diffusive behavior to shear-dominated convective behavior is well summarized in Fig. 8, which plots the viscosity vs. Péclet number for the 0.8% volume fraction dispersion at different shear rates in a single chart. In Stokesian dynamics studies of the shear thinning to shear thickening transition beyond a critical Péclet number, the transition Péclet number was achieved mainly by changing the shear

rate.[66] The critical Péclet number for the shear thinning to shear thickening transition is usually around $\mathrm{Pe}_{\mathrm{crit}}$ ~10 to 100 or even higher, depending on the interaction among particles.[67] By tuning both the shear rate and the temperature dependence of the base fluid viscosity, we can also clearly observe a similar transition for the suspension viscosity which first decreases with Péclet number and then increases with Péclet number (Fig. 8). Finally we note that if we define a relative viscosity $\eta_r = \frac{\eta(T,\dot{\gamma})}{\mu_s(T)}$ using the temperature-dependent base fluid viscosity, all of the data points shown in Fig. 8 at a given volume fraction collapse to a single master curve (which is shown in the inset of Fig. 8).

In summary, we have observed markedly different trends in the concentration-dependence of the shear viscosity and thermal conductivity of graphite suspensions below and above the percolation threshold. Below the percolation threshold, the thermal conductivity increases with volume fraction more rapidly with concentration than above the threshold, while the viscosity behaves in the inverse fashion. The increase in the thermal conductivity is found to be almost independent of temperature; however, the shear viscosity shows a complicated thermo-rheological behavior. Below the percolation threshold, the viscosity decreases with increasing temperature at all shear rates studied, while above the percolation threshold, the viscosity of

the percolated network initially increases with increasing temperature at low shear rates but this switches to a decreasing trend at high shear rates. The complicated thermal dependence of the shear viscosity can be understood by considering the Péclet number of the dispersion in conjunction with the evolution in the microstructure of the suspensions below and above the percolation threshold, which has been established through previous AC impedance spectroscopy studies. Below percolation, the graphite flakes form closely aggregated, isolated clusters. The diffusive Brownian contribution of these large clusters to the total viscosity is negligible. Above the percolation threshold, the surface energy of the isolated clusters is reduced and the diffusive motion of individual graphite flakes plus attractive interactions between the flakes become important. At low imposed shear rates, these interactions between the individual flakes and Brownian motion dominate and thus the viscosity increases with temperature. At high shear rates, the percolated network is disrupted, the particles are aligned by the flow and locally-advective hydrodynamic contributions to the total dissipation in the dispersion dominate the measured shear stress, leading to shear-thinning. The insights gained from this thermo-rheological study will help better understanding of structure-property relations of nanostructured dispersions. From an application viewpoint, our studies of both the viscosity and thermal

conductivity enhancements with nanoparticulate loading suggest that potential application of nanofluids in convective heat transfer should be focused on fluids below the percolation threshold as the shear viscosity (and thus the viscous energy dissipation) of the nanofluids and suspensions increases exponentially after crossing the percolation threshold, whereas the incremental gains from enhanced heat transfer are minimal.

Acknowledgements

The authors thank Dr. Thomas Ober for helpful discussion on the rheology measurements. This work is supported in part by US AFOSR FA9550-11-1-0174 (J.J.W. and G.C.). L.M. also gratefully acknowledges financial support from the National Natural Science Foundation of China (No. 51036003).

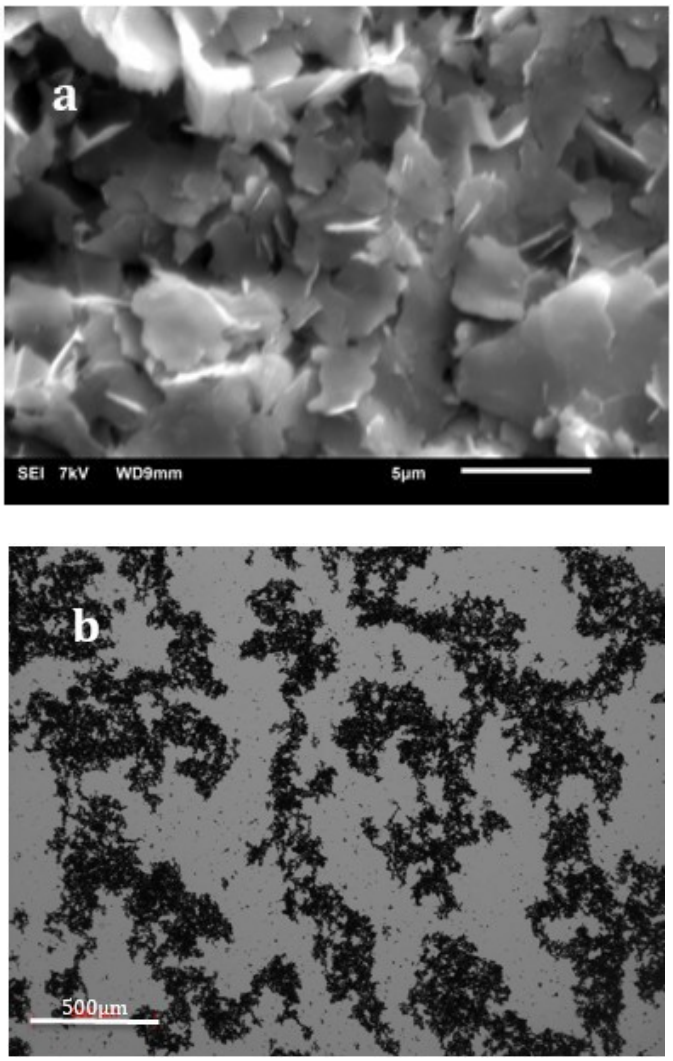

Figure 1: Microstructure of graphite flakes. (a) SEM image of individual graphite flakes in the dry state. (b) Optical image of a graphite suspension above the percolation threshold with volume fraction $\phi = 0.15\%$.

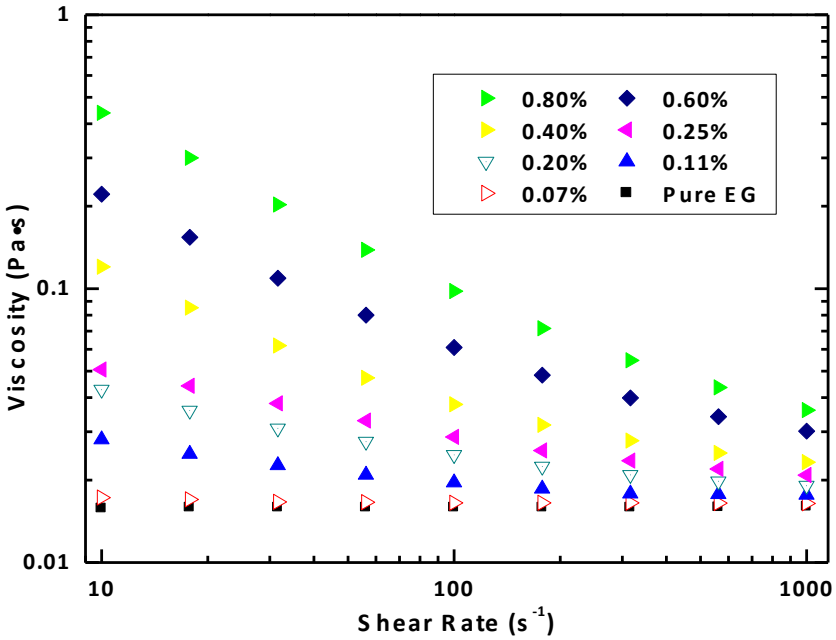

Figure 2: Viscosity of graphite-ethylene glycol suspensions with different volume fractions as a function of shear rate at room temperature. Non-Newtonian behavior (shear thinning) begins to dominate as the graphite volume fraction increases.

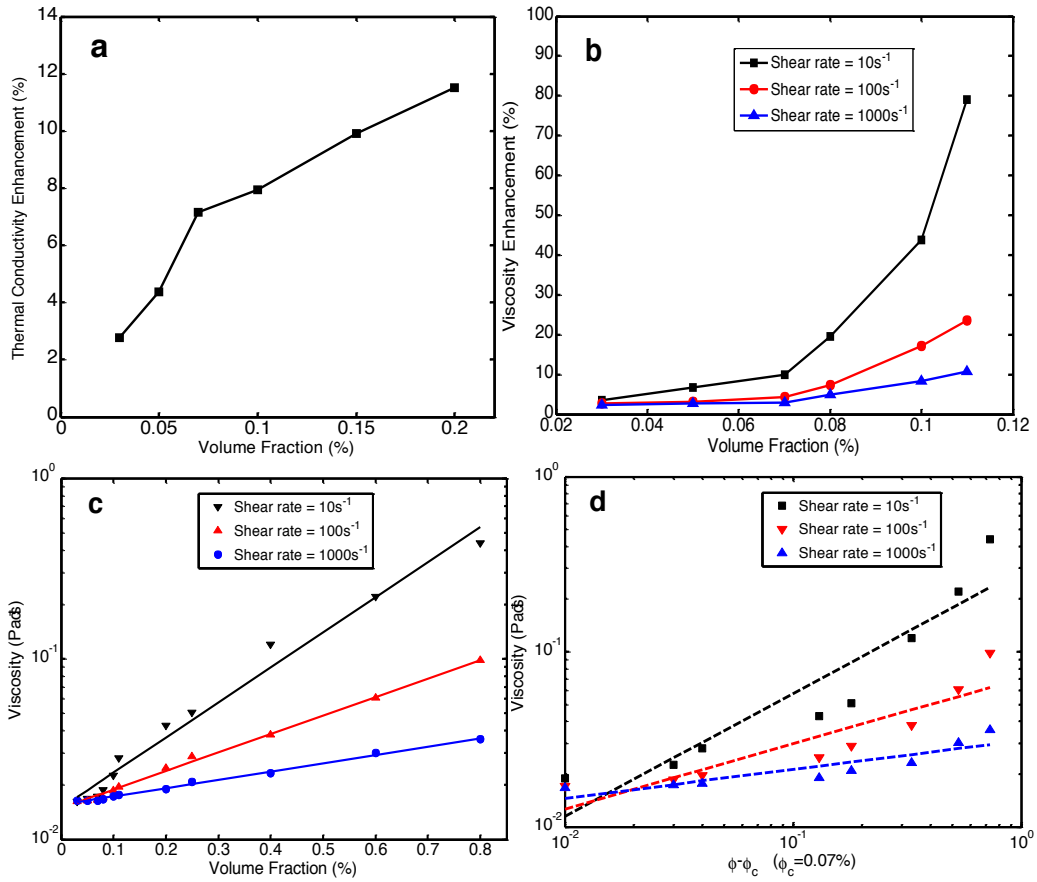

Figure 3: (a) Thermal conductivity enhancement of graphite suspensions as a function of volume fraction near the percolation regime. (b) Viscosity enhancement of graphite suspensions as a function of volume fraction near the percolation regime at given shear rates. (c) Viscosity as a function of volume fraction at different shear rates (=$10s^{-1}$, $100s^{-1}$, and $1000s^{-1}$). The solid lines are fitted using the Doolittle equation (the coefficients of determination R^2=0.9930, 0.9989, and 0.9962 for shear rate = $10s^{-1}$, $100s^{-1}$, and $1000s^{-1}$, respectively). (d) Viscosity after percolation as a function of volume fraction at different shear rates (=$10s^{-1}$, $100s^{-1}$, and $1000s^{-1}$). The dash lines are fitted using power law (the coefficients of determination R^2=0.6977, 0.7253, and 0.7786 for shear rate = $10s^{-1}$, $100s^{-1}$, and $1000s^{-1}$, respectively). The Doolittle equation fits much better than the power law.

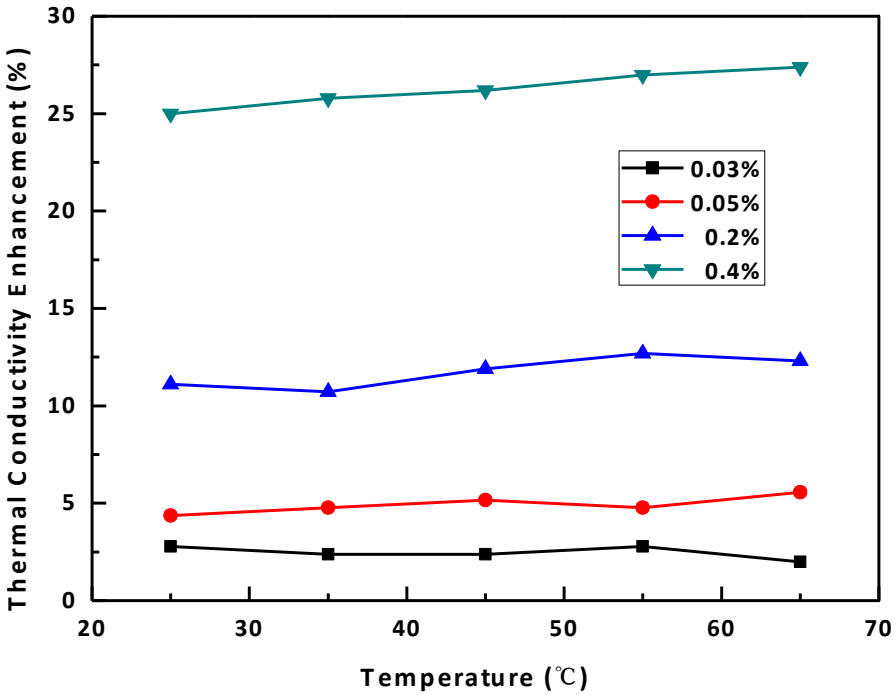

Figure 4: Thermal conductivity enhancement of graphite suspension as a function of temperature, showing that the enhancement is quite independent of temperature.

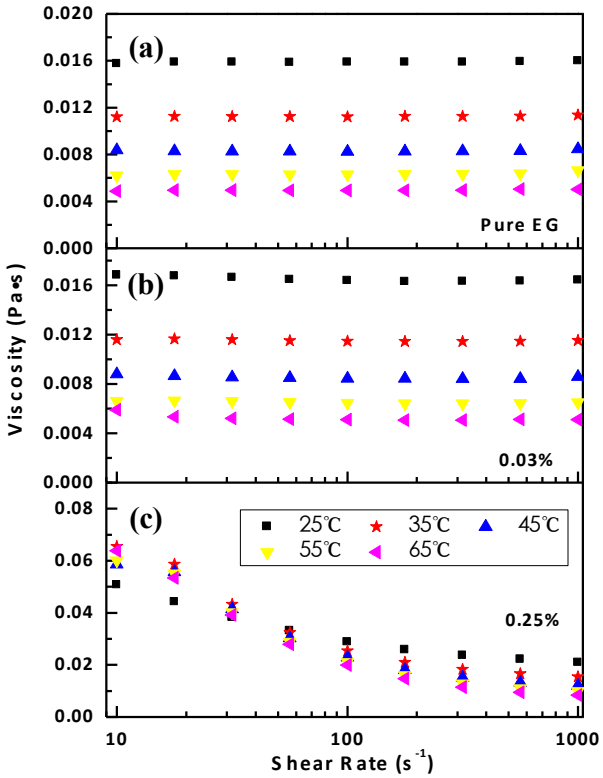

Figure 5: Steady shear viscosity of the graphite suspensions as a function of shear rate at different temperatures and different loadings. (a) pure ethylene glycol(EG); (b) graphite–ethylene glycol suspension with 0.03 vol% graphite loading; (c) graphite–ethylene glycol suspension with 0.25 vol% graphite loading.

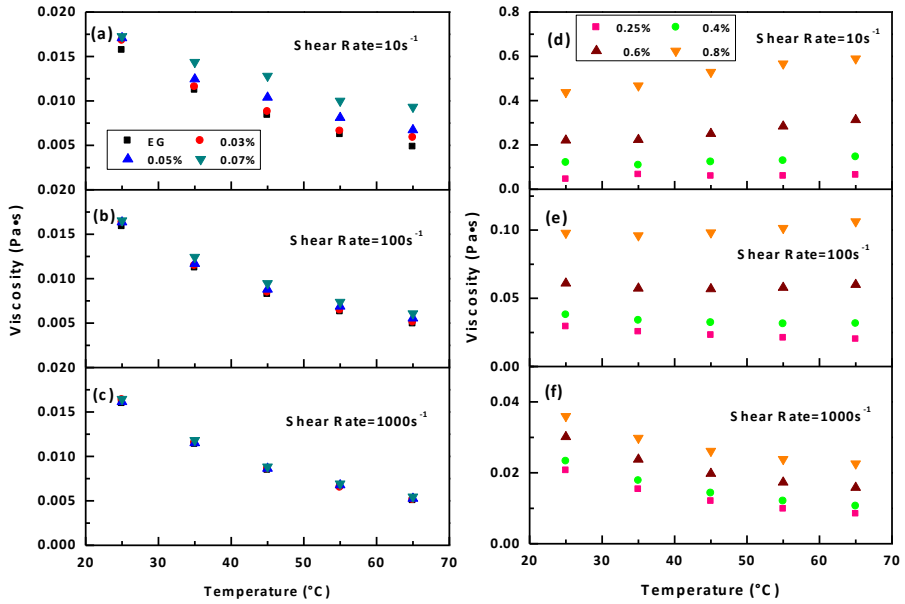

Figure 6: Viscosity as a function of temperature at different graphite volume fractions; (a)-(c) below percolation threshold, and (d)-(f) above percolation threshold. The temperature dependence of the viscosity changes above the percolation threshold from low shear rates to high shear rates.

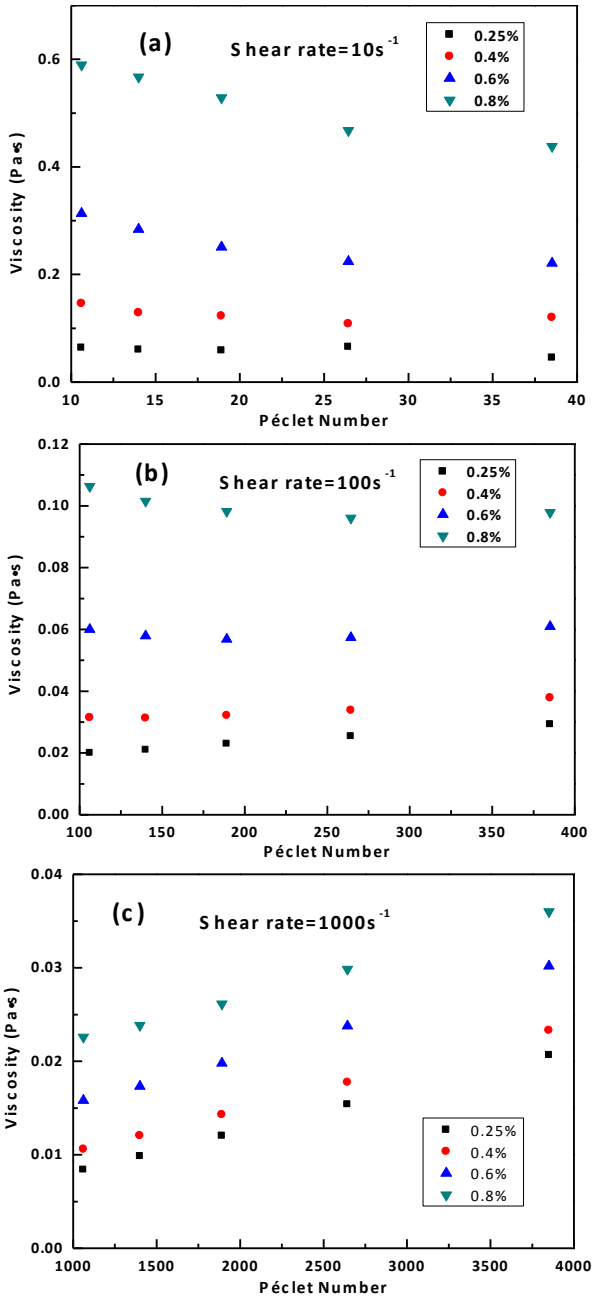

Figure 7: Viscosity of several suspensions at specified shear rates plotted as a function of the dimensionless Péclet number which is varied by increasing the temperature from 25℃ to 65℃.

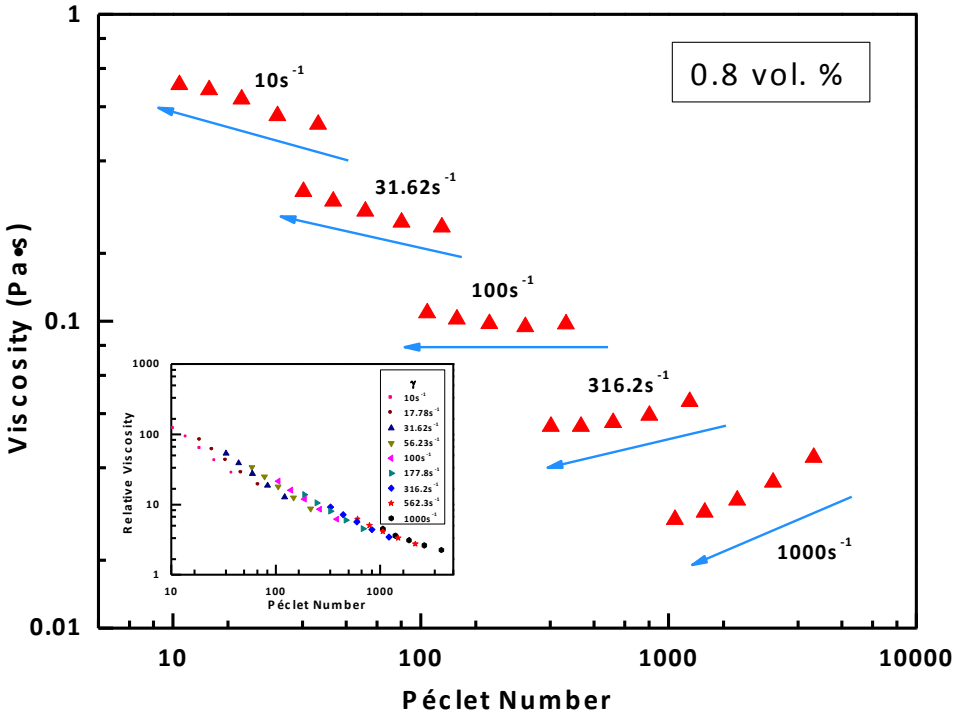

Figure 8: Viscosity as a function of Péclet number for 0.8 vol.% dispersion of graphite flakes at several characteristic shear rates. The arrow indicates the direction of temperature increases from 25℃ to 65℃. The inset shows that all the data points collapse to a single master curve when non-dimensionalizing the viscosity by the temperature dependent viscosity of the base fluid to give a relative viscosity $\eta_r = \eta(\dot{\gamma}, T)/\mu_s(T)$.

Bibliography

(1) Choi, S. U. S. *ASME Fluids Engineering Division* **1995,** 231, 99-106.
(2) Dhar, P.; Gupta, S. S.; Chakraborty, S.; Pattamatta, A.; Das, S. K. *Appl. Phys. Lett.* **2013,** 102, (16), 163114.
(3) Sastry, N. N. V.; Bhunia, A.; Sundararajan, T.; Das, S. K. *Nanotechnology* **2008,** 19, (5), 055704.
(4) Das, S. K.; Choi, S. U. S.; Yu, W.; T., P., *Nanofluids: Science and Technology*. Wiley-Interscience, 2007.
(5) Chandrasekar, M.; Suresh, S. *Heat Transfer Eng.* **2009,** 30, (14), 1136-1150.
(6) Kulkarni, D. P.; Vajjha, R. S.; Das, D. K.; Oliva, D. *Appl. Therm. Eng.* **2008,** 28, (14), 1774-1781.
(7) Wang, X.-Q.; Mujumdar, A. S. *Int. J. Therm. Sci.* **2007,** 46, (1), 1-19.
(8) Trisaksri, V.; Wongwises, S. *Renew. Sust. Energ. Rev.* **2007,** 11, (3), 512-523.
(9) Zhu, H.; Zhang, C.; Liu, S.; Tang, Y.; Yin, Y. *Appl. Phys. Lett.* **2006,** 89, (2), 23123-23123.
(10) Prasher, R.; Phelan, P. E.; Bhattacharya, P. *Nano Lett.* **2006,** 6, (7), 1529-1534.
(11) Philip, J.; Shima, P. D.; Raj, B. *Nanotechnology* **2008,** 19, (30), 305706.
(12) Karthikeyan, N. R.; Philip, J.; Raj, B. *Mater. Chem. Phys.* **2008,** 109, (1), 50-55.
(13) Jang, S. P.; Choi, S. U. S. *Appl. Phys. Lett.* **2004,** 84, (21), 4316-4318.
(14) Domingues, G.; Volz, S.; Joulain, K.; Greffet, J.-J. *Phys. Rev. Lett.* **2005,** 94, (8), 085901.
(15) Bhattacharya, P.; Saha, S. K.; Yadav, A.; Phelan, P. E.; Prasher, R. S. *J. Appl. Phys.* **2004,** 95, (11), 6492-6494.
(16) Gao, J.; Zheng, R.; Ohtani, H.; Zhu, D.; Chen, G. *Nano Lett.* **2009,** 9, (12), 4128-4132.
(17) Zheng, R.; Gao, J.; Wang, J.; Feng, S. P.; Ohtani, H.; Wang, J.; Chen, G. *Nano Lett.* **2012,** 12, (1), 188-192.
(18) López-Carranza, S. N.; Jenny, M.; Nouar, C. *C. R. Mecanique* **2012,** 340, (8), 602-618.
(19) Aravind, S. S. J.; Baskar, P.; Baby, T. T.; Sabareesh, R. K.; Das, S.; Ramaprabhu, S. *J. Phys. Chem. C* **2011,** 115, (34), 16737-16744.
(20) Venerus, D. C.; Buongiorno, J.; Christianson, R.; Townsend, J.; Bang, I. C.; Chen, G.; Chung, S. J.; Chyu, M.; Chen, H.; Ding, Y.; Dubois, F.; Dzido, G.; Funfschilling, D.; Galand, Q.; Gao, J.; Hong, H.; Horton, M.; Hu, L.; Iorio, C. S.; Jarzebski, A. B.; Jiang, Y.; Kabelac, S.; Kedzierski, M. A.; Kim, C.; Kim, J.-H.; Kim, S.; Mckrell, T.; Ni, R.; Philip, J.; Prabhat, N.; Song, P.; Vaerenbergh, S. V.; Wen, D.; Witharana, S.; Zhao, X.-Z.; Zhou, S.-Q. *Appl. Rheol.* **2010,** 20, (4).
(21) Chen, H.; Ding, Y.; Tan, C. *New J. Phys.* **2007,** 9, (10), 367.
(22) Duan, F.; Wong, T. F.; Crivoi, A. *Nanoscale Res. Lett.* **2012,** 7, (1), 1-6.
(23) Etemad, S. G.; Mujumdar, A. *Int. J. Heat Mass Tran.* **1995,** 38, (12), 2225-2238.
(24) Gingrich, W. K.; Cho, Y. I.; Shyy, W. *Int. J. Heat Mass Tran.* **1992,** 35, (11), 2823-2836.

(25) Malkin, A. Y. *J. Non-Newton. Fluid.* **2013,** 192, 48-65.
(26) Snijkers, F.; Pasquino, R.; Vermant, J. *Langmuir.* **2013,** 29, (19), 5701-5713.
(27) Yamaguchi, M.; Gogos, C. G. *Adv. Polym. Tech.* **2001,** 20, (4), 261-269.
(28) Liu, B.; Shangguan, Y.; Song, Y.; Zheng, Q. *J. Appl. Polym. Sci.* **2013,** 129, (3), 973-982.
(29) Koocheki, A.; Ghandi, A.; Razavi, S.; Mortazavi, S. A.; Vasiljevic, T. *Int. J. Food Sci. Tech.* **2009,** 44, (3), 596-602.
(30) Suzuki, S.; Uneyama, T.; Watanabe, H. *Macromolecules* **2013,** 46, (9), 3497-3504.
(31) Van de Ven, T. G. M.; Qasaimeh, M. A.; Paris, J. *Colloid Surface. A* **2004,** 248, (1), 151-156.
(32) Kole, M.; Dey, T. *J. Appl. Phys.* **2013,** 113, (8), 084307.
(33) Hojjat, M.; Etemad, S. G.; Bagheri, R.; Thibault, J. *Int. Commun. Heat Mass* **2011,** 38, (2), 144-148.
(34) Zhou, S.-Q.; Ni, R.; Funfschilling, D. *J. Appl. Phys.* **2010,** 107, (5), 054317.
(35) Duangthongsuk, W.; Wongwises, S. *Exp. Therm. Fluid. Sci.* **2009,** 33, (4), 706-714.
(36) Lee, J.-H.; Hwang, K. S.; Jang, S. P.; Lee, B. H.; Kim, J. H.; Choi, S. U. S.; Choi, C. J. *Int. J. Heat Mass Tran.* **2008,** 51, (11), 2651-2656.
(37) Nguyen, C. T.; Desgranges, F.; Roy, G.; Galanis, N.; Mare, T.; Boucher, S.; Angue Mintsa, H. *Int. J. Heat Fluid. Fl.* **2007,** 28, (6), 1492-1506.
(38) Snabre, P.; Mills, P. *J. Phys. III* **1996,** 6, (12), 1811-1834.
(39) Liu, D.-M. *J. Mater. Sci.* **2000,** 35, (21), 5503-5507.
(40) Xu, J.; Chatterjee, S.; Koelling, K. W.; Wang, Y.; Bechtel, S. E. *Rheol. Acta* **2005,** 44, (6), 537-562.
(41) Osuji, C. O.; Kim, C.; Weitz, D. A. *Phys. Rev. E* **2008,** 77, (6), 060402.
(42) Dhar, P.; Ansari, M. H. D.; Gupta, S. S.; Siva, V. M.; Pradeep, T.; Pattamatta, A.; Das, S. K. *J. Nanopart. Res.* **2013,** 15, (12), 1-12.
(43) Wei, T.; Fan, Z.; Luo, G.; Zheng, C.; Xie, D. *Carbon* **2009,** 47, (1), 337-339.
(44) Zheng, R.; Gao, J.; Wang, J.; Chen, G. *Nat. Commun.* **2011,** 2, 289.
(45) Yasmin, A.; Luo, J.-J.; Daniel, I. M. *Compos. Sci. Technol.* **2006,** 66, (9), 1182-1189.
(46) Wang, J. J.; Zheng, R. T.; Gao, J. W.; Chen, G. *Nano Today* **2012,** 7, (2), 124-136.
(47) Doolittle, A. K. *J. Appl. Phys.* **1951,** 22, (12), 1471-1475.
(48) Eapen, J.; Williams, W. C.; Buongiorno, J.; Hu, L.-W.; Yip, S.; Rusconi, R.; Piazza, R. *Phys. Rev. Lett.* **2007,** 99, (9), 095901.
(49) Evans, W.; Fish, J.; Keblinski, P. *Appl. Phys. Lett.* **2006,** 88, (9), 093116.
(50) Keblinski, P.; Cahill, D. G. *Phys. Rev. Lett.* **2005,** 95, (20), 209401.
(51) Bird, R. B.; Armstrong, R. C.; Hassager, O., *Dynamics of Polymeric Liquids. Vol. 1: Fluid Mechanics. 2nd Edition*. Wiley-Interscience, 1987.
(52) Reynolds, O. *Proceedings of the Royal Society of London* **1886,** 40, (242-245), 191-203.
(53) Jones, R. A., *Soft Condensed Matter*. Oxford University Press, 2002.
(54) Fulcher, G. S. *J. Am. Ceram. Soc.* **1925,** 8, (6), 339-355.
(55) Brown, E.; Jaeger, H. M. *J. Rheol.* **2012,** 56, (4), 875-923.
(56) Abbott, J.; Tetlow, N.; Graham, A.; Altobelli, S.; Fukushima, E.; Mondy, L.; Stephens, T. *J. Rheol.* **1991,** 35, (5), 773-795.
(57) Brinkman, H. *J. Chem. Phys.* **2004,** 20, (4), 571-571.

(58) Cheng, X.; McCoy, J. H.; Israelachvili, J. N.; Cohen, I. *Science* **2011,** 333, (6047), 1276-1279.
(59) Zarraga, I. E.; Hill, D. A.; Leighton Jr, D. T. *J. Rheol.* **2000,** 44, (2), 185-220.
(60) Brady, J. F.; Bossis, G. *Annu. Rev. Fluid. Mech.* **1988,** 20, 111-157.
(61) Bossis, G.; Brady, J. *J. Chem. Phys.* **1989,** 91, (3), 1866-1874.
(62) Foss, D. R.; Brady, J. F. *J. Fluid. Mech.* **2000,** 407, 167-200.
(63) Phung, T. N.; Brady, J. F.; Bossis, G. *J. Fluid. Mech.* **1996,** 313, 181-207.
(64) Sierou, A.; Brady, J. F. *J. Fluid. Mech.* **2001,** 448, 115-146.
(65) Larson, R. G., *The Structure and Rheology of Complex Fluids*. Oxford University Press, New York, 1999.
(66) Stickel, J. J.; Powell, R. L. *Annu. Rev. Fluid Mech.* **2005,** 37, 129-149.
(67) Wagner, N. J.; Brady, J. F. *Phys. Today* **2009,** 62, (10), 27-32.

Graphic for the Table of Contents